Biochimica et Biophysica Acta 1788 (2009) 1523–1533

Contents lists available at ScienceDirect

Biochimica et Biophysica Acta

journal homepage: www.elsevier.com/locate/bbamem

Membrane perturbation by the antimicrobial peptide PMAP-23: A fluorescence and molecular dynamics study

Barbara Orioni [a], Gianfranco Bocchinfuso [a], Jin Young Kim [b], Antonio Palleschi [a], Giacinto Grande [a], Sara Bobone [a], Yoonkyung Park [b,c], Jae Il Kim [d], Kyung-soo Hahm [b,c], Lorenzo Stella [a,*]

[a] Dipartimento di Scienze e Tecnologie Chimiche, Università di Roma Tor Vergata, Via della Ricerca Scientifica 1 00133 Roma, Italy
[b] Research Center for Proteineous Materials, Chosun University, 501-759 Gwangju, Republic of Korea
[c] Department of Cellular Molecular Medicine, Chosun University, 501-759 Gwangju, Republic of Korea
[d] Gwangju Institute of Science and Technology, Gwangju, Republic of Korea

ARTICLE INFO

Article history:
Received 23 February 2009
Received in revised form 3 April 2009
Accepted 13 April 2009
Available online 3 May 2009

Keywords:
Peptide–lipid interaction
Mechanism of antibacterial activity
Fluorescence spectroscopy
Depth-dependent quenching
Computer simulation

ABSTRACT

Several bioactive peptides exert their biological function by interacting with cellular membranes. Structural data on their location inside lipid bilayers are thus essential for a detailed understanding of their mechanism of action. We propose here a combined approach in which fluorescence spectroscopy and molecular dynamics (MD) simulations were applied to investigate the mechanism of membrane perturbation by the antimicrobial peptide PMAP-23. Fluorescence spectra, depth-dependent quenching experiments, and peptide-translocation assays were employed to determine the location of the peptide inside the membrane. MD simulations were performed starting from a random mixture of water, lipids and peptide, and following the spontaneous self-assembly of the bilayer. Both experimental and theoretical data indicated a peptide location just below the polar headgroups of the membrane, with an orientation essentially parallel to the bilayer plane. These findings, together with experimental results on peptide-induced leakage from large and giant vesicles, lipid flip-flop and peptide exchange between vesicles, support a mechanism of action consistent with the "carpet" model. Furthermore, the atomic detail provided by the simulations suggested the occurrence of an additional, more specific and novel mechanism of bilayer destabilization by PMAP-23, involving the unusual insertion of charged side chains into the hydrophobic core of the membrane.

1. Introduction

Antimicrobial peptides (AMPs) constitute a fundamental component of the innate immune defense [1,2], and have multiple functions, including immunomodulatory and chemotactic roles [3]. However, their mechanism of antibacterial activity is mainly based on association to the pathogen plasma membrane and perturbation of its permeability [2,4–7]. This is in marked contrast to traditional antibiotics, which usually act by attacking a specific receptor or enzymatic target, and it should significantly hinder the development of bacterial resistance to AMPs [8], since it is difficult for a microbe to change the phospholipid organization of its membrane. For this reason, AMPs are intensely investigated as a possible solution to the global problem of the insurgence of bacteria resistant to available antibiotic drugs [9,10]. Furthermore they also display interesting anticancer activity [11]. Even though several AMPs are already undergoing clinical trials [12–15], several issues need to be solved before they can find a widespread clinical application as systemic drugs, in particular regarding their toxicity, potential immunogenicity and rapid proteolytic degradation [14,16].

A detailed understanding of the mechanism of membrane destabilization by antimicrobial peptides is of paramount importance to design new analogues or peptide-mimicking molecules with improved activity, selectivity, and bioavailability properties, but such a molecular insight is still lacking. This is probably related to the difficulties involved in the application of the most powerful structural techniques (NMR and X-ray diffraction) to study peptide–membrane interactions [17]. Even though interesting progress is being made in the application of these techniques to AMPs [18–20], alternative approaches for gaining structural information in membranes would be desirable. Optical spectroscopies, and particularly fluorescence techniques, can be easily applied to model membrane systems, and even to live cells. They can provide a wealth of information on peptide–membrane interactions, such as peptide affinity for the membrane phase, its location and orientation in the bilayer, and its effects on membrane structure and integrity [21–27]. However, these low-resolution structural data are hardly sufficient for a clear structural interpretation of the pore-formation mechanism. On the

* Corresponding author. Tel.: +39 06 72594463; fax: +39 06 72594328.
E-mail address: stella@stc.uniroma2 (L. Stella).

0005-2736/$ – see front matter © 2009 Elsevier B.V. All rights reserved.
doi:10.1016/j.bbamem.2009.04.013

other hand, molecular dynamics (MD) simulations provide atomic-level data on the structure and dynamics of peptide–membrane systems [28,29,30,31], but they need a validation by comparisons with experimental data. We report here a combined approach, in which fluorescence spectroscopy experiments and MD simulations complement each other in the characterization of the interaction of PMAP-23 with lipid membranes.

PMAP-23 (RIIDLLWRVRRPQKPKFVTVWVR) [32] belongs to the group of cathelicidins, one of the major AMP families in mammals [33–35]. It shows a potent and broad spectrum antimicrobial activity against bacteria and fungi (due to membrane permeabilization), and it is not toxic to eukaryotic cells up to concentrations 100 times higher than those needed for bactericidal activity [36,37]. Its structure in membrane-mimicking environments has been determined by CD and NMR studies [38], and it appears to be an amphipathic helix, except for a central region, comprising the two Pro residues, which is disordered [39].

In order to obtain position-specific information from fluorescence spectroscopy experiments, two single-tryptophan analogues of PMAP-23 were synthesized, in which one of the two natural Trp residues was substituted by Phe. In the following, these analogues are indicated as W7 and W21, where the number indicates the position of the unmodified Trp.

Our results provide a clear picture of PMAP-23 location inside the bilayer and new insights in its membrane-destabilizing activity, including a possible functional role for the central non-helical segment, and a novel mechanism of bilayer perturbation involving the insertion of charged side chains into the hydrophobic membrane core.

2. Materials and methods

2.1. Materials

Phospholipids were purchased from Avanti Polar Lipids (Alabaster, AL), while carboxyfluorescein, Triton X-100, Sephadex G-50 and trypsin were purchased from Sigma (St. Louis, MO). Spectroscopic grade chloroform and methanol (C. Erba, Milan, Italy) were used.

2.2. Peptide synthesis

The peptides were synthesized using the solid-phase method with Fmoc [40]. Fmoc-protected peptides were deprotected and cleaved by incubation with a mixture of trifluoroacetic acid, phenol, water, thioanisole, and 1, 2-ethandithiol (82.5:5:5:5:2.5, v/v) for 3 h at room temperature. The synthetic peptides were purified by RP-HPLC on Shimadzu LC-6AD and Shimadzu LC-10Avp systems using an ODS column (4.6×250 mm). The purified peptides were shown to be homogeneous (>98%) by analytical HPLC. The molecular weight of all synthetic peptides was confirmed using Kratos Kompact matrix-assisted laser desorption/ionization time-of-flight mass spectrometry (MALDI-TOF MS, Shimadzu, Japan).

2.3. Liposome preparation

Large unilamellar vesicles were prepared as previously described [22]. All liposomes were formed by egg phosphatidylcholine (ePC) and egg phosphatidylglycerol (ePG) (2:1 molar ratio). This lipid mixture has been widely used to mimic bacterial membranes; even though PC is not a bacterial lipid, this composition reproduces the content of zwitterionic and anionic lipids in the cytoplasmic membrane of bacteria. Lipids were hydrated in a 10 mM phosphate buffer (pH 7.4), containing 140 mM NaCl and 0.1 mM EDTA. Total lipid concentration is reported.

Liposomes containing the fluorescent lipid 1-palmitoyl-2-[6-((7-nitrobenz-2-oxa-1,3-diazol-4-yl)amino)caproyl]-L-α-phosphatidylcholine (C6-NBD-PC) were prepared essentially as described in [26]. A 5% (mol/mol) ratio was used between labeled and total lipids. Chemical quenching by sodium dithionite [41,42] was obtained with a 1500:1 dithionite:NBD molar ratio.

The degree of labeling of nitroxide-containing lipids (1-palmitoyl-2-stearoyl(n-doxyl)-sn-glycero-3-phosphocholine, with $n=5$, 7, 10, 12, 14, 16, and 1,2-diacyl-sn-glycero-3-phosphotempocholine), employed for depth-dependent quenching studies, was determined by double integration of electron paramagnetic resonance (EPR) spectra [43]. nitroxide-labeled liposomes were produced by adding the labeled lipids to the initial chloroform solution (7% molar fraction). Spin label content was controlled directly on the final liposomes by double integration of the EPR spectra of an aliquot of the liposomes dissolved in isopropanol. All liposome preparations contained the same amount of spin labels, within a 10% error. The fluorescent peptide analogs were added to the different nitroxide-labeled liposomes (at a lipid concentration of 0.2 mM) and to a reference unlabeled liposome solution, and steady-state fluorescence intensities were determined after a 20 min equilibration period. The reported values are the average of triplicate experiments.

Giant unilamellar vesicles (GUVs) were prepared by the electroformation method, as previously described [44], in a 0.3 M sucrose, 3 μM carboxyfluorescein (CF) solution. A 1.5 V (peak to peak), 10 Hz potential was applied to the electroformation chamber, for 1 h, and then switched to 4 V, 4 Hz for 15 min to favor detachment of GUVs from the electrode. The solution contained in the electroformation chamber was gently removed, and diluted 300 times in buffer (pH7.4, 10 mM phosphate, 140 mM NaCl, 0.1 mM EDTA). The lipid composition of GUVs was 66% ePC, 33% ePG and 1% rhodamine-labeled phosphatidylethanolamine (Rho-PE). Silanized glass slides were employed during fluorescence imaging. The GUVs content and the lipid membrane could be observed independently by imaging the green CF fluorescence and the red Rho-PE fluorescence.

2.4. Leakage mechanism

Peptide-induced membrane permeability was determined by measuring the fractional release of CF entrapped inside liposomes, as already reported [22]. In order to determine the leakage mechanism (graded or “all or none”), the quenching efficiency of the carboxyfluorescein still entrapped inside vesicles after partial peptide-induced leakage was measured. Different peptide concentrations (10 to 15 μM) were incubated with ePC/ePG vesicles (lipid concentration 200 μM), containing 30 mM CF for different times, in order to obtain various levels of partial leakage. The peptide was then digested by trypsin addition (final concentration 50 μg/mL), and this immediately stopped the leakage process (within the few seconds needed for sample mixing), indicating that complete peptide digestion had been achieved, and that PMAP-23 proteolytic fragments did not retain any membrane activity. The CF released until trypsin addition was separated from the vesicles by gel permeation chromatography. The quenching efficiency (E) of the CF still entrapped inside vesicles was determined by comparing the fluorescence intensity of intact vesicles (F) with that measured after the same vesicles were disrupted by adding the detergent Triton X-100, 1 mM (F_0): $E=1-F/F_0$. In order to determine the dependence of the quenching efficiency on the CF concentration entrapped inside vesicles, liposomes (50 μM lipid concentration) with different known internal CF concentrations (between 5 and 30 mM) were prepared, and the quenching efficiency determined as described above.

2.5. Fluorescence spectroscopy

Steady-state fluorescence experiments were carried out on a SPEX Fluoromax 2 fluorimeter (Edison, NJ). Temperature was controlled to

25 °C by a thermostatted cuvette holder. Peptide fluorescence was excited at 280 nm.

2.6. Water–membrane partition

The peptide fraction associated to the lipid bilayers of liposomes ($x_{membrane}$) was determined by the variation of fluorescence intensity observed following peptide partition from the water to the membrane phase, according to the following equation

$$F(\lambda) = x_{membrane}F_{membrane}(\lambda) + (1 - x_{membrane})F_{water}(\lambda)$$

where $F_{membrane}$ and F_{water} are the fluorescence intensities measured when the peptide is in one phase only.

The average wavelength of the peptide emission spectrum was calculated according to the following equation:

$$\langle\lambda\rangle = \frac{\int\lambda \cdot F(\lambda)d\lambda}{\int F(\lambda)d\lambda}$$

where the integral was extended from 320 to 420 nm.

2.7. Peptide exchange between vesicles

Experiments of peptide exchange between different vesicles were carried out by incubating the peptide (5 μM) with vesicles labeled with the fluorescent lipid N-NBD-PE (1,2-dioleoyl-sn-glycero-3-phosphoethanolamine-N-(7-nitro-2-1,3benzoxadiazol-4-yl), which quenches the intrinsic peptide tryptophan fluorescence by acting as an energy-transfer acceptor (lipid 200 μM). Peptide exchange between vesicles was monitored by measuring the decrease in energy transfer following addition of unlabeled vesicles (final concentration 800 μM). Fluorescence intensity was recorded with an excitation wavelength of 280 nm.

2.8. Lipid flip-flop

Vesicles labeled in the inner layer with C6-NBD-PC (lipid concentration 200 μM) were incubated for 20 min with different concentrations of PMAP-23, to cause peptide-induced lipid flip-flop. Successively, the peptide was digested by incubating with 2 μM of trypsin for 10 min, to remove any peptide-induced membrane pores. The amount of C6-NBD-PC translocated across the membrane bilayer was determined by adding sodium dithionite, and following NBD reduction by the decrease of fluorescence intensity. NBD fluorescence was excited at 460 nm and monitored at 520 nm. Results are reported as flip-flop fractions, where complete flip-flop corresponds to the attainment of an equilibrium distribution of labeled lipids in the two membrane layers.

2.9. Molecular dynamics simulations

Molecular dynamics simulations were performed according to the method proposed by Esteban-Martín and Salgado [45]. Briefly, PMAP-23 was initially shaped in a canonical α-helix, with extended side chains, and positioned at the center of a cubic box with a side of 8.5 nm. 32 POPG molecules (16 molecules for each of the two possible chiralities of POPG) and 96 POPC molecules, with different conformations taken from equilibrated simulations of phospholipid bilayers [46], and then 5026 water molecules were added randomly in the box. Finally, 26 Na^+ ions were introduced in substitution of 26 randomly selected water molecules, to ensure system neutrality. MD simulations were performed with GROMACS 3.3, using *ffgmx* parameters [47]. The simple point charge (SPC) model was used for water [48], and water geometry was constrained with the SETTLE algorithm [49]. POPC and POPG parameters were previously reported [50–52]. A Berendsen thermostat, with a coupling constant of 0.1 ps, was applied in all simulations [53]. The reference temperature was set to 300 K, except where stated otherwise. Pressure coupling was applied anisotropically, also employing the Berendsen scheme, with a time constant of 1.0 ps and a reference pressure of 1 bar. Bond lengths were constrained with the LINCS algorithm [54]. Short-range electrostatics and Lennard–Jones interactions were cut-off at 1.0 nm and long range electrostatic interactions were calculated by using the particle mesh Ewald algorithm [55,56]. Simulations were run with a 4 fs timestep, removing fast hydrogen vibrations according to Feenstra et al. [57]. The system was energy-minimized and a first 100 ps equilibration MD run was performed with position restraining on the peptide. Molecular graphics were obtained with the program VMD [58].

3. Results

3.1. Membrane-perturbing activity

The membrane-perturbing activity of PMAP-23 and its analogues was determined by measuring the peptide-induced leakage of the fluorescent tracer carboxyfluorescein (CF) entrapped inside phospholipid vesicles (Fig. 1). Both single-tryptophan PMAP-23 analogues exhibited a membrane-perturbing activity comparable to the natural peptide, in agreement with previous findings showing that their antimicrobial activity on several different bacterial strains was comparable [39]. Therefore, the two analogues W7 and W21 could be employed as reliable models of the behavior of PMAP-23.

Giant unilamellar vesicles (GUVs), whose size is in the micrometers range, allowed direct visualization of the peptide-induced leakage process by fluorescence microscopy experiments (Fig. 2). The lipid membrane and the aqueous contents of the vesicles were imaged simultaneously by taking advantage of the green fluorescence of entrapped carboxyfluorescein and of the red emission of a rhodamine-labeled lipid, respectively. PMAP-23 was able to cause the leakage of vesicle contents, as indicated by the disappearance of CF emission caused by its diffusion in the extravesicular volume. However, no observable changes took place in the membrane, even after complete release of GUV contents, indicating that PMAP-23 causes membrane leakage by forming pores rather than by causing membrane micellization.

Another important question regarding the release mechanism is whether it takes place as an “all-or-none” or as a graded process. In the

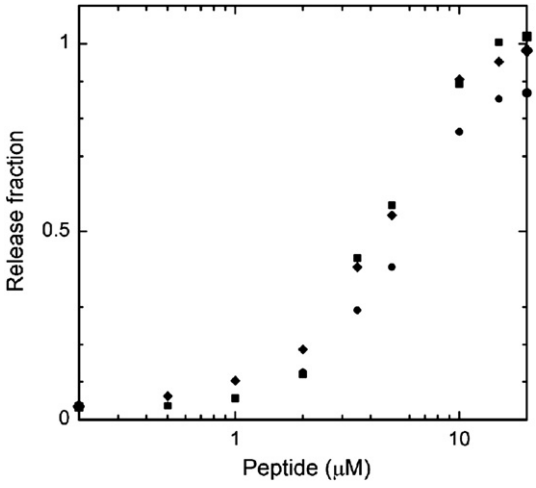

Fig. 1. Fraction of overall liposome contents released after addition of different peptide concentrations. Leakage was determined by the variation of carboxyfluorescein emission intensity following release from the liposome's internal volume. Liposome composition ePC/ePG 2:1 (mol/mol). Lipid concentration 0.2 mM. Diamonds PMAP-23; squares W7; circles W21.

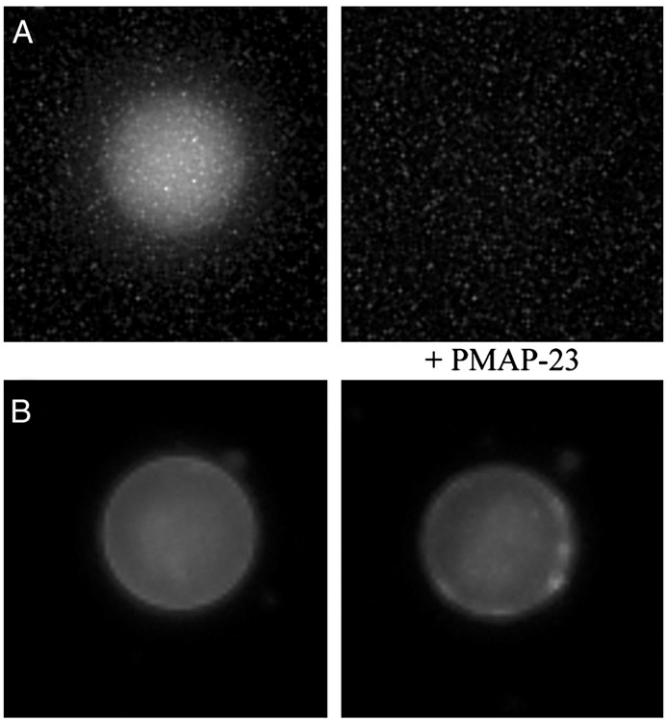

Fig. 2. Fluorescence microscopy images of PMAP-23 induced leakage from a giant unilamellar vesicle. Panel A: fluorescence emission from carboxyfluorescein molecules entrapped inside the GUV, before and after peptide addition. The fluorophore was completely released. Panel B: fluorescence emission from rhodamine-labeled phospholipids located in the GUV bilayer. The membrane remained intact even after complete release of the GUV contents. The vesicle diameter is about 20 μm.

first case only completely full and completely empty vesicles are present in the sample at a given time during the leakage kinetics, since the time needed for the leakage of liposome contents is shorter than the lifetime of peptide-induced pores. By contrast, in the case of a graded leakage, partially emptied vesicles are present [59]. The two possibilities can be discriminated by measuring the carboxyfluorescein quenching efficiency after partial peptide-induced leakage has taken place [60,61], thanks to the fact that self quenching of CF is due to dye aggregation, and therefore it is strongly concentration dependent [62]. Fig. 3A shows the CF self-quenching efficiency measured for different CF concentration entrapped inside ePC/ePG vesicles. The quenching efficiency E was satisfactorily described by a phenomenological Hill sigmoidal curve defined by the equation

$$E = \frac{(KC)^n}{1 + (KC)^n}$$

with $n = 1.5$ and $K = 76.2\ M^{-1}$, in agreement with previous reports on similar systems [60–62].

In the case of an all-or-none mechanism, at any time during the leakage process each vesicle is either completely empty or it contains the same CF concentration originally entrapped inside the liposomes. Therefore, the self-quenching efficiency of entrapped CF is always the same, irrespective of the fraction of vesicles that have released their contents. On the other hand, in a graded process, the CF concentration inside the liposomes decreases during the leakage, causing a decrease in the self-quenching efficiency of entrapped CF [60].

PMAP-23 was incubated with CF-containing liposomes for different times, in order to obtain various levels of partial leakage. The leakage process was stopped by digesting the peptide with trypsin and the released CF was separated from the vesicles by gel permeation chromatography. The self-quenching efficiency of the CF still entrapped inside vesicles was always constant within experimental errors (Fig. 3B), demonstrating that the leakage process followed an all-or-none mechanism.

3.2. Peptide-induced lipid flip-flop

In the absence of external perturbations the rate of spontaneous translocation of lipids across the bilayer (lipid "flip-flop") is so low that several days are needed until an initially asymmetric membrane attains a homogeneous lipid distribution in both layers. However, many membrane-perturbing agents cause a huge enhancement of this rate, so that the flip-flop process can be completed even in a few minutes [63].

In order to check whether PMAP-23 induces lipid translocation across the two leaflets of the membrane, vesicles labeled with the fluorescent lipid C6-NBD-PC (1-palmitoyl-2-[6-((7-nitrobenz-2-oxa-1,3-diazol-4-yl)amino)caproyl]-L-α-phosphatidylcholine) in the inner leaflet of the membrane only were incubated with different concentrations of PMAP-23. The peptide was then digested by trypsin addition, and the fraction of labeled lipids translocated to the external layer was determined by measuring their quenching by sodium

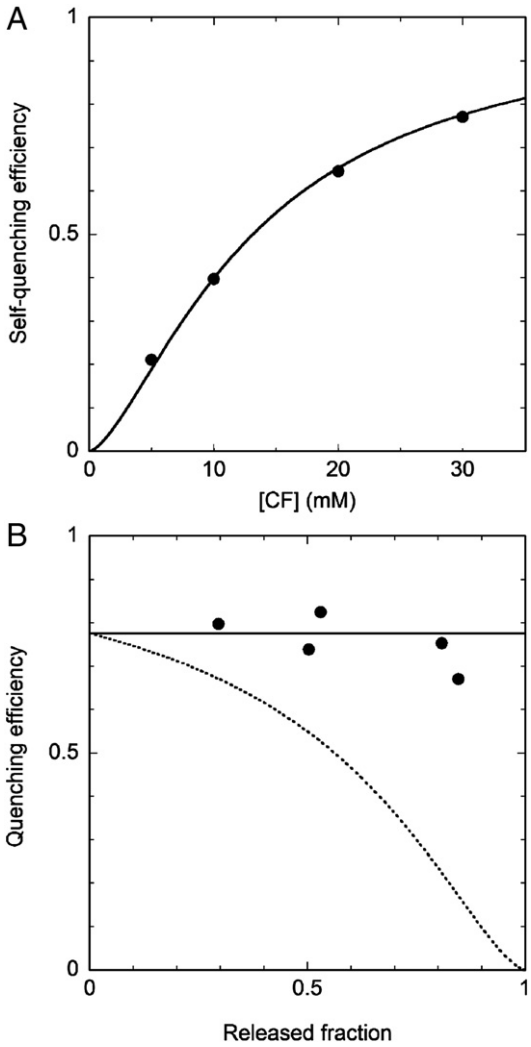

Fig. 3. Panel A: Concentration dependence of self-quenching efficiency for CF entrapped inside ePC/ePG vesicles. Panel B: CF self-quenching efficiency after partial PMAP-23 induced leakage. Peptide-induced leakage from ePC/ePG vesicles containing 30 mM CF was stopped after the release of different fractions of CF contents by digesting PMAP-23 with trypsin. The continuous curve represents the constant quenching value expected for an all-or-none leakage mechanism, while the broken curve shows the quenching efficiency expected in the case of graded release (according to the concentration dependence of the self-quenching efficiency determined from the data in panel A).

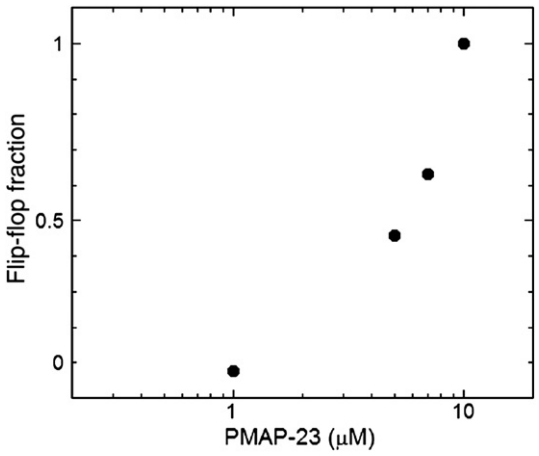

Fig. 4. Fraction of lipids flip-flopped across the membrane during 20 min of incubation with different concentrations of PMAP-23.

dithionite [64]. A significant peptide-induced lipid flip-flop was observed (Fig. 4). Interestingly, this phenomenon exhibited a dependence on peptide concentration very similar to that observed in the leakage curves (Fig. 1), suggesting that the two phenomena are coupled.

3.3. Water–membrane peptide partition

We next investigated peptide partition between the water and membrane phase of PMAP-23 and its analogues, by measuring the changes in peptide fluorescence caused by titration of a peptide solution with phospholipid vesicles. As shown in Fig. 5, the three analogues exhibited a comparable affinity for membranes, with a complete binding at lipid concentrations higher than 150 μM. Also the spectral shift caused by membrane association was similar for the three peptides (Fig. 5B), suggesting that the two Trp residues of PMAP-23 sensed a similar environment when the peptide was bound to the membrane.

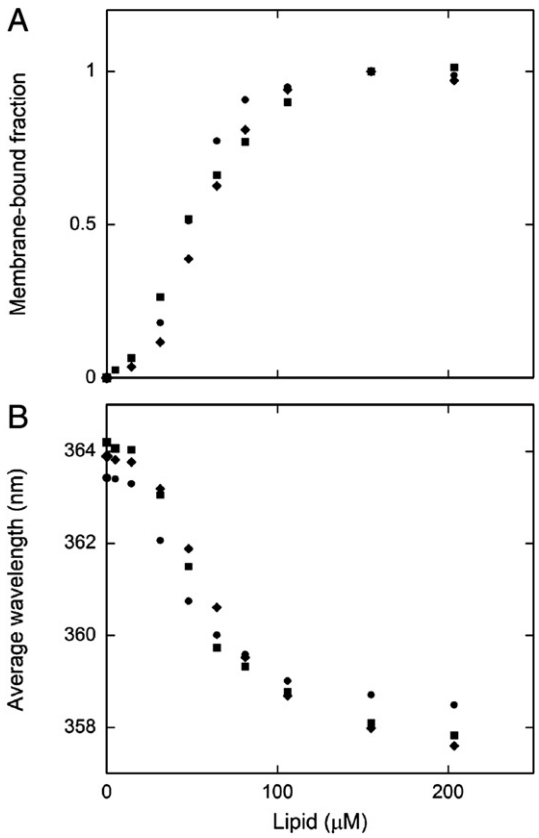

Fig. 5. Panel A: Water-membrane partition curves of PMAP-23, W7, and W21. Panel B: Variation in the average wavelength of the emission spectra of the three analogues caused by membrane binding. PMAP-23 (diamonds), W7 (squares) and W21 (circles). Liposome composition ePC/ePG 2:1 (mol/mol). Peptide concentration 10 μM.

3.4. Peptide location in the bilayer

A more precise determination of peptide location in the membrane could be obtained by depth-dependent quenching experiments [65]. Fig. 6 shows the peptide-fluorescence quenching caused by association to liposomes containing lipids labeled at different depths along the acyl chain with a nitroxide group, which acted as a quencher of peptide tryptophan fluorescence. Surprisingly, the quenching profile was rather wide and ill defined, as compared to similar experiments performed on other peptides [26,27,66–69], particularly in the case of Trp7. However, the quenching curves for both single-fluorophore analogues show a maximum slightly below 1 nm from the bilayer center.

3.5. Peptide exchange between vesicles

The ability of PMAP-23 to exchange between different vesicles was assessed by a method based on fluorescence resonance energy transfer (FRET). The peptide was added to vesicles labeled with the fluorescent lipid N-NBD-PE (1,2-Dioleoyl-sn-Glycero-3-phosphoethanolamine-N-(7-nitro-2-1,3benzoxadiazol-4-yl), which can act as a FRET acceptor for the intrinsic peptide tryptophan fluorescence. Peptide and lipid concentrations (5 μM and 200 μM, respectively) were chosen to ensure complete peptide association to the vesicles. After equilibration of the system, an excess of unlabeled vesicles (final concentration 800 μM) was added to the sample. A spectral change was observed, which was completed within the few seconds needed for mixing and acquisition: Trp fluorescence increased and NBD emission decreased (Fig. 7), indicating a reduced FRET efficiency caused by peptide exchange between acceptor-labeled and unlabeled vesicles. Under this respect it is worth mentioning that the time-scale

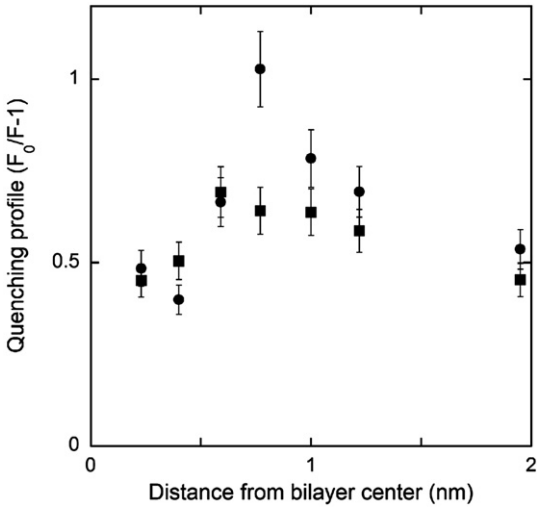

Fig. 6. Depth-dependent quenching experiments. The ordinate values ("quenching profile") represent values of $F_0/F-1$, where F_0 is the fluorescence intensity of peptides associated to unlabeled liposomes, and F is the emission intensity of the peptide bound to vesicles labeled with quenching groups located at different distances from the bilayer center. Peptide concentration 1 μM, lipid concentration 200 μM. Squares: W7; circles: W21.

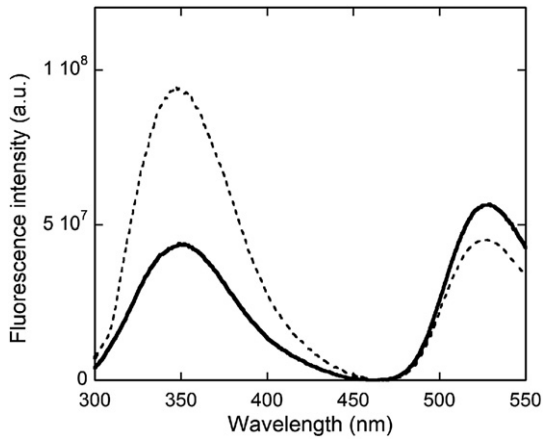

Fig. 7. FRET experiment demonstrating the ability of PMAP-23 to exchange between different vesicles. The continuous curve represents the emission spectrum ($\lambda_{exc.}$ 280 nm) of a sample in which the peptide (5 μM) was added to ePC/ePG vesicles labeled with C6-NBD-PC. The broken line is the spectrum of the same sample immediately after addition of an excess of unlabeled vesicles. The decrease in FRET efficiency between Trp residues and NBD, caused by the passage of PMAP from labeled to unlabeled vesicles, is demonstrated by the increase in Trp fluorescence ($\lambda_{max.}$ ~350 nm) and the concomitant decrease in NBD emission ($\lambda_{max.}$ ~520 nm).

of intervesicular transfer of the fluorescent lipid is orders of magnitudes slower [70].

3.6. Peptide translocation across the bilayer

A FRET assay [26] was employed to determine whether the peptide, when added to a vesicle suspension, would remain associated to the outer layer of the liposomes or translocate across the membrane to become distributed in the whole bilayer. An energy-transfer acceptor for Trp fluorescence was introduced in the liposomes as a fluorescent lipid (C6-NBD-PC). Two different types of vesicles were prepared: outer layer labeled liposomes (OL), where the fluorescent probe was incorporated only in the outer layer by adding it to a vesicle suspension after liposome formation and inner layer labeled liposomes (IL), obtained by chemically quenching the label in the outer layer of liposomes homogeneously labeled in both layers. The FRET phenomenon has an inverse sixth power dependence on distance, with a 50% quenching efficiency at an interprobe distance called the Förster radius [71,72]. In the case of the Trp-NBD pair, this distance is 26 Å [21], whereas the thickness of the bilayer is approximately 40 Å [73]. Since the fluorophore of C6-NBD-PC is located in the region of the polar headgroups [74–76], a peptide lying in the outer layer or a peptide distributed in the whole bilayer would be quenched quite differently. In the case of PMAP-23 a significant energy transfer was observed only with OL liposomes (Fig. 8), indicating that the peptide did not translocate across the membrane, at least at the concentration investigated. It is important to note that this assay can only be performed under conditions in which lipid asymmetry is conserved, and lipid flip-flop is negligible during the assay time. For this reason, the experiment could only be performed at 1 μM PMAP-23 concentration, at which the peptide is not active (see above).

3.7. Molecular dynamics simulations

In order to further characterize PMAP-23 position in the bilayer, molecular dynamics (MD) simulations were performed following a novel *minimum bias* approach. Present day computational resources allow simulation of large systems (such as those including a hydrated lipid bilayer) for times in the 0.1–1 μs range. However, these trajectory lengths are not sufficient for a complete sampling of all possible peptide arrangements in the relatively viscous environment of a preformed membrane bilayer [28,77]. As a result, simulations of peptide interaction with lipid membranes can be influenced significantly by the starting conditions, being unable to find the global free energy minimum. Recently, an approach to overcome this limitation based on the spontaneous self-assembly of lipid bilayers has been proposed [45,78]. In this case, simulations starting from a random mixture of lipids, water, and one peptide molecule lead to the spontaneous formation of a bilayer membrane in a computationally accessible time (10–100 ns). During this self-assembly process (which involves intermediate steps where the lipid and water phase start to separate long before an ordered bilayer is formed) the peptide is able to position in the most favorable local environment, taking advantage of the high fluidity of the system. It is interesting to note that, at the best of our knowledge, the present study is the first case in which a quantitative test of the MD results obtained with this approach is attempted, taking advantage of our depth-dependent quenching experiments, and of previously reported NMR and CD studies [38].

Two independent simulations were performed in order to test the reliability of the results, with the peptide initially forced in a perfect α-helical conformation, but with different initial random configurations of water and lipids. In 100 ns of simulation a lipid bilayer formed in both cases, although a rather stable water-filled pore was still present (Fig. 9), as previously observed in all simulations of spontaneous bilayer formation [78,79–81]. To facilitate elimination of bilayer defects, the system was cycled repeatedly between 300 K and 375 K (rising the temperature linearly in 2 ns, decreasing it in 50 ps, and keeping it constant at 300 K for 950 ps). This annealing protocol did not cause significant modifications in peptide conformation or position. After the water channel was eliminated (i.e. after 13 and 27 cycles in the two simulations), the trajectory was extended for further 10 ns keeping the temperature at 300 K. All data analyses were performed on these final trajectory segments, which were deemed equilibrated as judged from the root mean square positional displacements of the peptide atoms, from the stability of the peptide secondary structure, from the membrane thickness and molecular surface area (data not shown), and from the density map of phosphorus atoms and peptide backbone atoms (see below).

A representative frame of one of the two simulations is shown in Fig. 10A, illustrating PMAP-23 position inside the bilayer; a very similar arrangement was observed in both simulations. The peptide

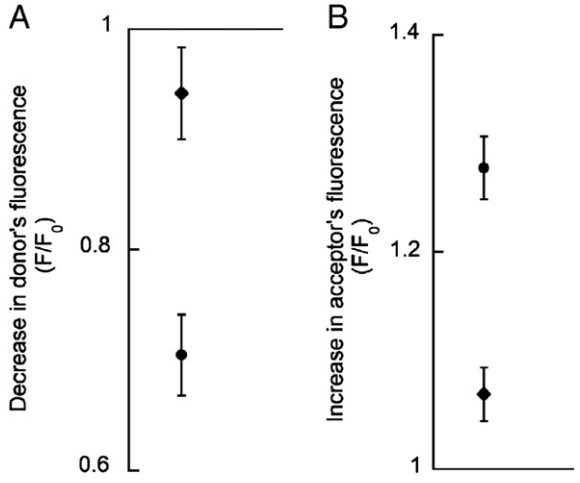

Fig. 8. FRET experiments on peptide translocation. Panel A: decrease in PMAP-23 fluorescence (F) when NBD-labeled lipids, acting as FRET acceptors, were added to the outer or to the inner leaflet of the liposome membrane, with respect to the fluorescence of PMAP-23 associated to unlabeled vesicles (F_0). Panel B: increase in NBD fluorescence (F) when the peptide was added to liposomes containing the fluorescent lipid in the outer or inner leaflet of the membrane, with respect to the fluorescence measured in the absence of PMAP-23 (F_0). Data referring to outer layer labeled liposomes are represented by circles, while those referring to inner layer labeled liposomes are shown as diamonds. PMAP-23 concentration 1 μM, lipid concentration 200 μM.

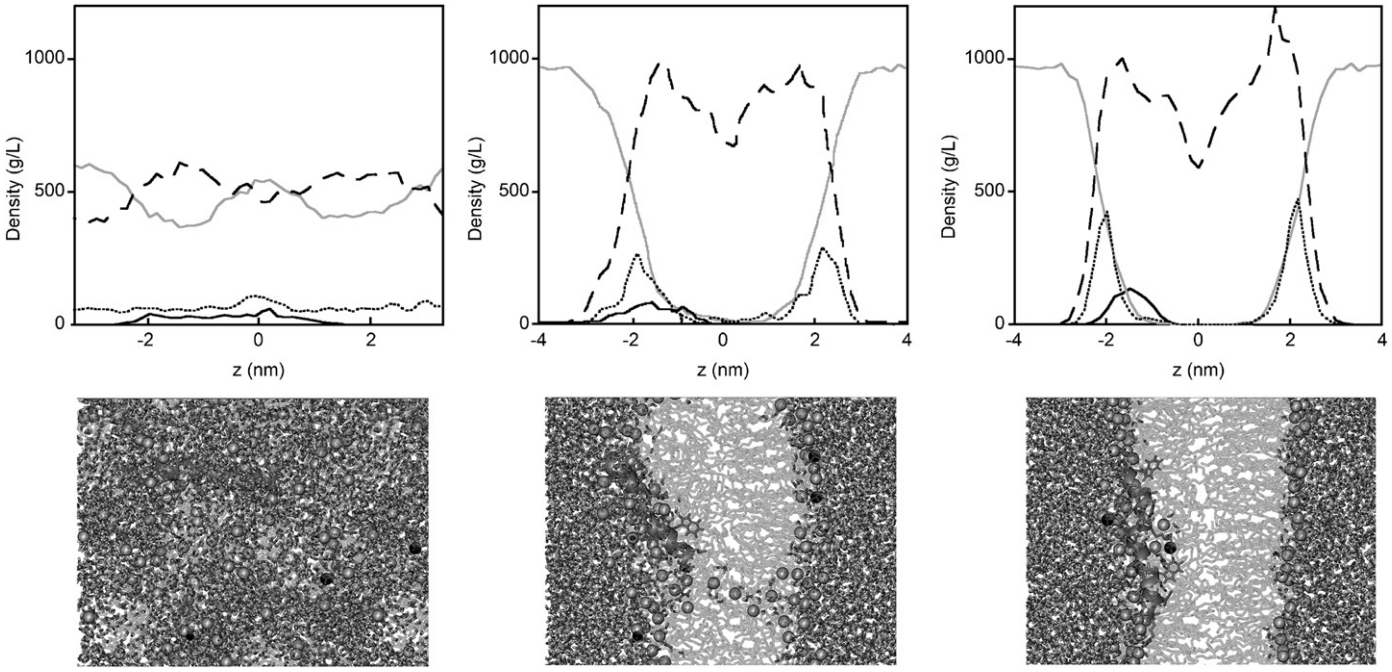

Fig. 9. Bilayer formation during the MD simulation. Left, center and middle panels represent, respectively, the situation after the initial restrained simulation, after 100 ns of unrestrained simulation, and at the end of the trajectory, after bilayer defects were removed with an annealing protocol. The density distribution graphs shown in the upper panels indicate the position of water molecules (gray line), phospholipids (dashed line), peptide (black solid line) and phosphate groups (dotted line).

lied parallel to the membrane surface, at the interface between the polar and apolar regions. The positional distribution of the indole moieties of both Trp residues was centered at about 1 nm from the bilayer center (Fig. 10B), in agreement with the fluorescence experiments. The helical conformation of the peptide was substantially maintained, but a significant discontinuity was observed in correspondence of the central segment (where the two Pro residues are located), in agreement with previous NMR experiments in detergent micelles [38]. In this conformation, the peptide side chains were arranged in an amphiphilic orientation, but two of the charged side chains (Arg10 and Lys14) were forced in the apolar side. Interestingly, these side chains were inserted in the lipid core of the membrane, and caused a significant perturbation by forcing some lipid polar heads and water molecules deep inside the bilayer (Fig. 10A). This perturbation was stably maintained for all the final segments of the trajectories, as demonstrated by the density map calculated for the peptide backbone atoms and for the lipid phosphorus atoms during the last 10 ns of the trajectories (Fig 10C).

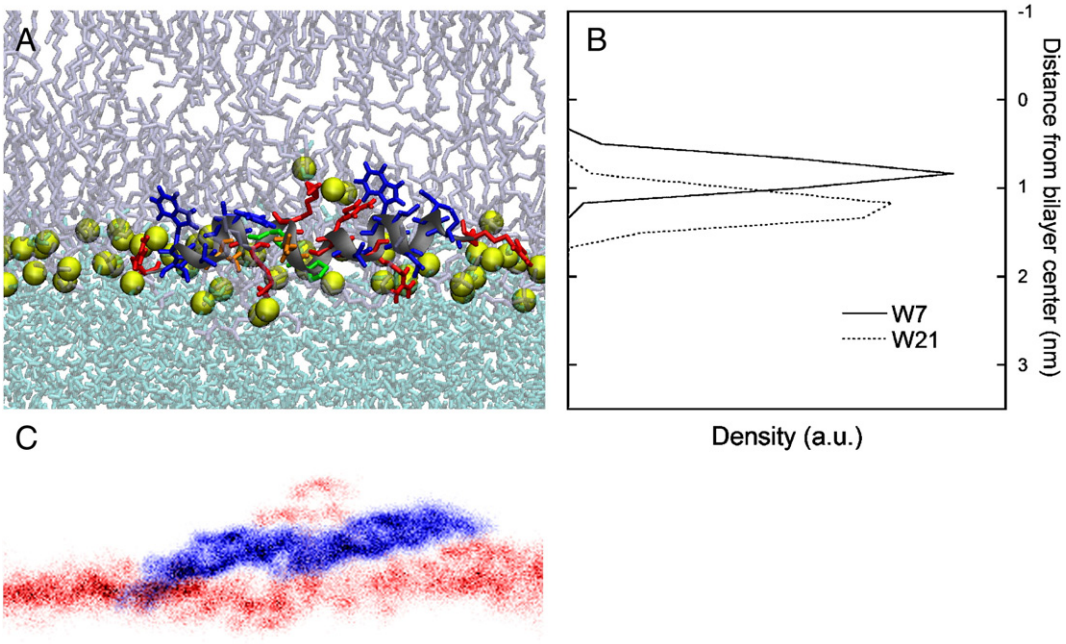

Fig. 10. Panel A: Representative structure at the end of one of the two MD simulations. Water is represented in cyan, phospholipids in gray, and phospholipids' phosphorus atoms as yellow spheres. The peptide backbone is shown in grey, charged side chains in red, polar aminoacids in orange, apolar residues in blue, and prolines in green. Panel B: Density distribution of the indole moieties of the two Trp residues of PMAP-23 in the same MD simulation, averaged over the trajectory segment after formation of a defect-free bilayer. Panel C: Density map of the lipid phosphorus atoms (red) and of the peptide backbone atoms (blue) averaged over the last 10 ns of the trajectory.

The disorder caused by peptide association to the membrane was assessed by determining the order parameters of the palmitic chains of the lipids with respect to the bilayer normal [82] during the last 10 ns of the trajectory. The average order parameter in the lipid leaflet not containing PMAP-23 was 0.45 and 0.44 in the two simulations, while the same parameter calculated in the membrane layer including the peptide was significantly reduced (0.32 and 0.29). Furthermore, the average order parameter of the lipids whose polar heads where drawn in the apolar region of the bilayer by association to the charged side chains of Arg10 and Lys 14 was −0.02 and 0.15 in the two simulations, demonstrating a specific disordering effect of these peptide residues.

4. Discussion

Peptide–membrane interactions play a prominent role in many biological processes, such as bilayer translocation by cell-penetrating peptides [83], peptide-induced membrane fusion [84], fibril formation by amyloid peptides [85], and membrane destabilization by AMPs. However, a thorough understanding of all these phenomena is still elusive, mainly due to difficulties involved in the structural studies of peptide–membrane systems. The determination of the structure of membrane proteins is notoriously difficult, since these molecules rarely form crystals suitable for X-ray diffraction, and their incorporation in model membranes hinders high resolution structural studies by multidimensional NMR techniques. As a consequence, membrane proteins account for less than 2% of records included in the Protein Data Bank [86]. Pores constituted by antimicrobial peptides present even additional difficulties due to the intrinsic dynamical nature of these systems. For instance, the first determination by X-ray diffraction of the electron density profile of an AMP channel was only recently reported, but the resolution was intrinsically limited by the variability of the pore position within the periodic cell and by the variability of atomic positions within the pore structure [20].

Molecular dynamics simulations can be applied to such systems, and provide the positions of all atoms and their dynamical behavior. However, due to the approximations involved in the computations, they need to be validated by comparisons with experimental data to be deemed reliable. To this end, we have compared MD results with several fluorescence spectroscopy experiments, which supplement previously published NMR and CD data on peptide conformation [38]. Such a combined application of spectroscopic experiments and computational data has previously proved valuable in our studies on the solution structure of peptide foldamers [71,87–90] and on protein dynamics [91–93], but its application to peptide–membrane interactions has been very limited so far [94].

In the case of the antimicrobial peptide PMAP-23, our fluorescence data clearly indicated a peptide orientation essentially parallel to the membrane plane, and an approximate location just below the polar headgroups of the bilayer. The two Trp residues located at different positions along the primary sequence exhibited comparable spectral shifts as a consequence of membrane association. Since Trp emission is strongly dependent on its insertion depth inside a membrane [95,96], this finding suggests a similar location of the two residues in the bilayer. Furthermore, depth-dependent quenching experiments confirmed that both Trp residues were located preferentially at about 1 nm from the bilayer center, i.e. at a depth corresponding approximately to the interface between the polar headgroups region and the hydrophobic core of the bilayer (Fig. 9). The depth of insertion and orientation observed here for PMAP-23 are similar to those of other AMPs of the same family, such as LL-37 [97,98]. In connection to the depth-dependent quenching experiments, it is interesting to note that the dependence of the quenching efficiency on the depth of the quenching group was less peaked than those previously observed for other peptides [26,27,66–69], particularly for Trp7. In order to interpret this result, it is important to consider that the observed quenching profile results from the convolution of the distribution of depths populated both by the fluorophore and by the quencher [66]. Therefore, the broad quenching profile observed for PMAP-23 could be attributed to two possible causes: the peptide might sample a wide distribution of depths inside the bilayer [23], or, alternatively, peptide binding could induce local disorder in the phospholipids, increasing the width of the depth distribution sampled by the quenching moieties. MD results clearly indicated the second effect as the dominant one, as further discussed below.

Fluorescence data provided also further indications regarding the distribution of PMAP-23 between the two leaflets of the membrane, showing that it was not able to translocate across the bilayer, at least at concentrations at which it was still not causing membrane leakage. This is in contrast with the behavior of other, more hydrophobic AMPs, such as trichogin, which form transmembrane pores and which can distribute in both membrane layers even at concentrations at which they are not active [26].

MD results were in excellent agreement with all the available experimental evidences. In both trajectories, the helical character of the peptide conformation was essentially retained, in agreement with CD data showing that PMAP-23 is mostly helical when associated to lipid membranes [38]. However, the helical structure was lost in the central segment of the peptide comprising Pro 12 and 15, and this allowed a much more amphiphilic arrangement of the side chains than in the perfect helical structure which was used as the starting conformation in our simulations. In this final membrane-bound conformation all the apolar residues pointed towards one side of the helix, and most of the charged side chains were located on the opposite side. An amphiphilic distribution of the side chains is a common feature of helical [99] and non-helical AMPs [100], and strongly favors their interaction with the membrane surface. However, an exception to the regular amphiphilic distribution of the side chains in the conformation attained during the simulations was provided by two charged residues (Arg10 and Lys14) located close to the central kink, which pointed towards the apolar face of the peptide helix. All of the main structural features of the conformation attained during the simulations (helical character, with a break in the central segment, and amphiphilic arrangement of the side chains with the exception of Arg10 and Lys14, which point towards the apolar face) are in agreement with the PMAP-23 structure previously determined by NMR experiments in membrane-mimicking micelles [38].

In addition to peptide conformation, also its position in the bilayer during the MD simulations was in good agreement with the available experimental data: in both trajectories, the helix was oriented essentially parallel to the membrane plane, and located just below the region of the phosphate moieties, in conformity with the fluorescence data reported above. Overall, these findings support the view that the self-assembling, minimum-bias simulative approach employed in this study can be deemed a reliable method to determine peptide structure inside phospholipid membranes.

More interestingly, the MD simulations allowed us to investigate the effects of peptide binding on the lipid bilayer organization (at low peptide to lipid ratios). When PMAP-23 was associated to the lipid bilayer in our simulations, the side chains of Arg10 and Lys 14 became deeply inserted into the hydrophobic core of the membrane. This finding might seem surprising, since the transfer of charged groups from a polar solvent (such as water) to an apolar environment (such as the core of a lipid bilayer) is strongly unfavorable [101,102]. However, this side-chain arrangement appears to be imposed by the peculiar features of PMAP-23: Arg10 takes part in a helical segment comprising also Arg8 and Arg11, and it would be impossible for these three charged side chains to point all towards the same side of the helix. Similarly, Lys14 is strongly constrained, being located between Pro12 and Pro15, which is then followed by another Lys residue. Notwithstanding the forced imperfect amphiphlic arrangement of the charged side chains, peptide association to the phospholipid bilayer is

ensured by the high membrane affinity of the two amphiphilic helical segments: the Wimley and White hydrophobicity scale for interfacial peptide partitioning [103] predicts a free energy of water–membrane partition of −5.6 and −4.7 kcal/mol for the PMAP-23 helical segments 1–11 and 15–23, respectively. These values are more than sufficient to counterbalance the free energy cost related to the insertion of Arg10 and Lys14: for these two residues, the Wimley and White water–octanol hydrophobicity scale [103] predicts values of 1.8 and 2.8 kcal/mol, respectively, for membrane insertion, and similar values are reported in the "biological" hydrophobicity scale of Hessa et al. [104]. Furthermore, our simulations suggest that the high free energy penalty associated with the dehydration of the charged side chains was strongly reduced by local bilayer deformations, which allowed the interaction of the Arg and Lys residues with lipid polar headgroups and water molecules drawn inside the bilayer. This finding is in agreement with other recent MD simulations, showing that Lys and Arg side chains, when forced inside lipid bilayers, always cause such local perturbations [77,101,105–111]. In addition, it had been previously shown that salt-bridge formation (in our case between the peptide side chains and the charged phosphatidylglycerol headgroups) can reduce the free energy cost of desolvating charged groups [112].

It is important to note that in our classical MD simulations the protonation state of the charged groups was fixed during the whole trajectory. Therefore, it may be argued that the observed deformations in the bilayer structure were due to the *a priori* assumption of a charged state for the Lys and Arg side chains, even when located inside the hydrophobic lipid core where their pKa might change significantly. However, recent free energy calculations showed that Lys and Arg residues remain protonated even when inserted at significant depths inside the membrane [101,108,109,111].

Interestingly, the local disorder caused in the lipid bilayer by the insertion of two charged side chains provides also an explanation for the ill-defined depth-dependent quenching profiles observed for Trp7 of PMAP-23, which is located close to the lipid region disordered by Arg10 and Lys 14 (Fig. 10).

Our fluorescence microscopy experiments with giant vesicles have shown that PMAP-23 causes the leakage of membrane contents with the formation of pores, and this appears to be the mechanism of its antimicrobial activity. It is worth to consider the possible implications of the observed effects of PMAP-23 on the structure of the bilayer for the mechanism of its membrane-perturbing activity, also in view of other experimental evidences. Different models were proposed for the mechanism of pore formation by antimicrobial peptides [7], but except for subtle differences, they fall essentially in two classes [113]. The "barrel-stave" model [114] predicts the formation of well defined pores by several peptide helices which aggregate in a transmembrane orientation, like the staves in a barrel, with their hydrophilic face lining the water-filled pore lumen, and the hydrophobic side oriented towards the lipid membrane. A typical representative for AMPs acting through this mechanism is the peptaibol alamethicin [23]. On the other hand, in the alternative mechanism, commonly termed the "carpet model" [4,8,115–117], peptides accumulate on the external membrane surface (like a carpet), causing expansion of the outer layer and a strain between the two leaflets of the bilayer. When a threshold local concentration is reached, this strain is released through the formation of local membrane defects, which could involve the formation of toroidal pores, in which the lipid bilayer folds back onto itself in a doughnut shape [118]. Several cationic AMPs appear to act according to this model [4]. The observed location of PMAP-23 on the membrane surface clearly points to the second mechanism of membrane perturbation. This conclusion is further supported by the correlation of peptide-induced membrane leakage with lipid translocation (flip-flop), since the formation of local defects in the membranes can promote the exchange of lipids between the two membrane layers [63,116].

The consensus view of the mechanism of membrane disruption through this model is based on the effects of peptide insertion on the surface tension of the external membrane layer [119]. However, our MD results suggest an additional, more specific mechanism of bilayer destabilization, involving the insertion of charged side chains into the hydrophobic core of the membrane, while the peptide is lying at the water–membrane interface. This mechanism has never been observed before, and definitely it does not apply generally to helical cationic AMPs, since a survey of about 50 Protein Data Bank structures of antimicrobial peptides determined by NMR spectroscopy in membrane-mimicking environments did not evidence any other peptide in which a few charged side chains point decidedly towards the apolar face of the helix. However, this does not exclude the possibility that the membrane perturbation mechanism observed in the present study might be of relevance also for other membrane-active peptides, in addition to PMAP-23. For instance, a recent NMR study by Hong et al. [120] indicated that Arg side chains of the β-hairpin antimicrobial peptide protegrin-1, while inserted into the hydrophobic part of the bilayer, are closely associated to the phosphate groups of membrane phospholipids. A similar interaction has also been proposed to mediate the membrane translocation of cell-penetrating peptides [107].

During our simulations (which involved a single peptide), the actual formation of membrane defects leading to the diffusion of water from one side to the other of the bilayer, was not observed. However, the perturbation induced by a single peptide chain was sufficient to cause water penetration deep inside the membrane. It can be hypothesized that when several peptides accumulate on the bilayer surface in close proximity, the cumulative effects of charged side chains insertion in the bilayer on its structure could easily lead to the formation of a local membrane defect, or pore. Such a cooperative effect is supported by the observation that the carboxyfluorescein leakage caused by PMAP-23 followed an all-or-none mechanism, in which the liposomes remained full until a lesion formed and all their contents were rapidly released. This finding is consistent with the view in which the perturbation caused by isolated PMAP-23 molecules is not sufficient to cause leakage, and therefore a local accumulation of bound peptide is needed for the formation of a membrane pore. This conclusion is further supported by the observation that in our leakage experiment a complete release of the contents of all liposomes was obtained only at a bound peptide to lipid ratio of 1/10 (Fig. 1). Since the area occupied by a peptide molecule can be estimated from our MD structure to be around 400 $Å^2$ and the area per lipid molecule is about 70 $Å^2$ [121], this peptide/lipid ratio corresponds to an almost complete coverage of the membrane surface.

In conclusion, a coupled approach employing fluorescence experiments and molecular dynamics simulations can be successfully used to characterize the interaction of bioactive peptides with lipid membranes. Fluorescent data are essential to validate the simulative results, and the good agreement observed in the present study between the computational and experimental data suggests that determination of peptide location inside lipid bilayers by state of the art simulative methods can be reliable. This opens the way for a new understanding of the mechanism of action of AMPs, since MD simulations provide a structural detail unattainable by any presently available experimental method. In the case of PMAP-23, combined experimental and simulative data support the carpet model for mechanism of membrane perturbation, but indicate as well that this peptide causes membrane destabilization also in a more specific way, by introducing two charged side chains deep into the hydrophobic membrane core. Further experiments are now underway on PMAP-23 analogues to confirm this hypothesis.

Acknowledgements

This paper is dedicated to Prof. B. Pispisa, on the occasion of his retirement.

This project was supported by the Italian Ministry of Foreign Affairs, the Italian Ministry of University and Research (PRIN 2006) and by the Korea Foundation for International Cooperation of Science & Technology (KIKOS) (K20713000012-07B0100-01210). Computational resources were kindly made available by the Fermi and CASPUR Research Centers (Rome). We thank Prof. J. Z. Pedersen for the EPR determinations of doxyl label content, and Prof. B. Pispisa, Prof. Y. Kim and Dr. C. Mazzuca for helpful discussions.

References

[1] R.E.W. Hancock, H.G. Sahl, Antimicrobial and host-defense peptides as new anti-infective therapeutic strategies, Nat. Biotechnol. 24 (2006) 1551–1557.
[2] A. Giuliani, G. Pirri, A. Bozzi, A. Di Giulio, M. Aschi, A.C. Rinaldi, Antimicrobial peptides: natural templates for synthetic membrane-active compounds, Cell Mol. Life Sci. 65 (2008) 2450–2460.
[3] K.L. Brown, R.E.W. Hancock, Cationic host defense (antimicrobial) peptides, Curr. Opin. Immunol. 18 (2006) 24–30.
[4] Y. Shai, Mode of action of membrane active antimicrobial peptides, Biopolymers 66 (2002) 236–248.
[5] H. Sato, J.B. Feix, Peptide–membrane interactions and mechanism of membrane destruction by amphipatic α-helical antimicrobial peptides, Biochim. Biophys. Acta 1758 (2000) 1245–1256.
[6] H.W. Huang, Molecular mechanism of antimicrobial peptides: the origin of cooperativity, Biochim. Biophys. Acta 1758 (2006) 1292–1302.
[7] B. Bechinger, K. Lohner, Detergent-like actions of amphipathic cationic antimicrobial peptides, Biochim. Biophys. Acta 1758 (2006) 1529–1539.
[8] M. Zasloff, Antimicrobial peptides of multicellular organisms, Nature 415 (2002) 389–395.
[9] R.P. Wenzel, M.B. Edmond, Managing antibiotic resistance, N. Engl. J. Med. 343 (2000) 1961–1963.
[10] O. Cars, L. Diaz Högberg, M. Murray, O. Nordberg, S. Sivaraman, C. Stålsby Lundborg, A.D. So, G. Tomson, Meeting the challenge of antibiotic resistance, Br. Med. J. 337 (2008) a1438.
[11] D.W. Hoskin, A. Ramamoorthy, Studies on anticancer activities of antimicrobial peptides, Biochim. Biophys. Acta 1778 (2008) 357–375.
[12] A.R. Koczulla, R. Bals, Antimicrobial peptides: current status and therapeutic potential, Drugs 63 (2003) 389–406.
[13] E. Andrès, J.L. Dimarcq, Cationic antimicrobial peptides: update of clinical development, J. Int. Med. 255 (2004) 519–520.
[14] A.K. Marr, W.J. Gooderham, R.E.W. Hancock, Antibacterial peptides for therapeutic use: obstacles and realistic outlook, Curr. Opin. Pharmacol. 6 (2006) 468–472.
[15] M. Zaiou, Multifunctional antimicrobial peptides: therapeutic targets in several human diseases, J. Mol. Med. 85 (2007) 317–329.
[16] L. M. Gottler, A. Ramamoorthy, Structure, membrane orientation, mechanism, and function of pexiganan — a highly potent antimicrobial peptide designed from magainin. Biochim. Biophys. Acta. In press, doi:10.1016/j.bbamem.2008.10.009
[17] J.J. Lacapère, E. Pebay-Peyroula, J.M. Neumann, C. Etchebest, Determining membrane protein structures: still a challenge! Trends Biochem. Sci. 32 (2007) 259–270.
[18] M. Hong, Structure, topology, and dynamics of membrane peptides and proteins from solid-state NMR spectroscopy, J. Phys. Chem. B 111 (2007) 10340–10351.
[19] F. Porcelli, B.A. Buck-Koehntop, S. Thennarasu, A. Ramamoorthy, G. Veglia, Structures of the dimeric and monomeric variants of magainin antimicrobial peptides (MSI-78 and MSI-594) in micelles and bilayers, determined by NMR spectroscopy, Biochemistry 45 (2006) 5793–5799.
[20] S. Qian, W. Wang, L. Yang, H.W. Huang, Structure of the alamethicin pore reconstructed by X-ray diffraction analysis, Biophys. J. 94 (2008) 3512–3522.
[21] L.M.S. Loura, R.F.M. de Almeida, A. Coutinho, M. Prieto, Interaction of peptides with binary phospholipid membranes: application of fluorescence methodologies, Chem. Phys. Lipids 122 (2003) 77–96.
[22] L. Stella, C. Mazzuca, M. Venanzi, A. Palleschi, M. Didonè, F. Formaggio, C. Toniolo, B. Pispisa, Aggregation and water–membrane partition as major determinants of the activity of the antibiotic peptide Trichogin GA IV, Biophys. J. 86 (2004) 936–945.
[23] L. Stella, M. Burattini, C. Mazzuca, A. Palleschi, M. Venanzi, C. Baldini, F. Formaggio, C. Toniolo, B. Pispisa, Alamethicin interaction with lipid membranes: a spectroscopic study on synthetic analogues, Chem. Biodivers. 4 (2007) 1299–1312.
[24] L. Stella, M. Venanzi, K.S. Hahm, F. Formaggio, C. Toniolo, B. Pispisa, Shining a light on peptide-lipid interactions: fluorescence methods in the study of membrane-active peptides, Chem. Today 26 (2008) 44–46.
[25] A.E. Johnson, Fluorescence approaches for determining protein conformations, interactions and mechanisms at membranes, Traffic 6 (2005) 1078–1092.
[26] C. Mazzuca, L. Stella, M. Venanzi, F. Formaggio, C. Toniolo, B. Pispisa, Mechanism of membrane activity of the antibiotic trichogin GA IV: a two-state transition controlled by peptide concentration, Biophys. J. 88 (2005) 3411–3421.
[27] E. Gatto, C. Mazzuca, L. Stella, M. Venanzi, C. Toniolo, B. Pispisa, Effect of peptide lipidation on membrane perturbing activity: a comparative study on two trichogin analogues, J. Phys. Chem. B. 110 (2006) 22813–22818.
[28] E. Matyus, C. Kandt, D.P. Tieleman, Computer simulation of antimicrobial peptides, Curr. Med. Chem. 14 (2007) 2789–2798.
[29] H. Khandelia, J.H. Ipsen, O.G. Mouritsen, The impact of peptides on lipid membranes, Biochim. Biophys. Acta 1778 (2008) 1528–1536.
[30] H. Leontiadou, A.E. Mark, S.J. Marrink, Antimicrobial peptides in action, J. Am. Chem. Soc. 128 (2006) 12156–12161.
[31] D. Sengupta, H. Leontiadou, A.E. Mark, S.-J. Marrink, Toroidal pores formed by antimicrobial peptides show significant disorder, Biochim. Biophys. Acta 1778 (2008) 2308–2317.
[32] M. Zanetti, P. Storici, A. Tossi, M. Scocchi, R. Gennaro, Molecular cloning and chemical synthesis of a novel antimicrobial peptide derived from pig myeloid cells, J. Biol.Chem. 269 (1994) 7855–7858.
[33] L. Tomasinsig, M. Zanetti, The cathelicidins — structure, function and evolution, Curr. Protein Pept. Sci. 6 (2005) 23–34.
[34] I. Zelezetsky, A. Pontillo, L. Puzzi, N. Antcheva, L. Segat, S. Pacor, S. Crovella, A. Tossi, Evolution of the primate cathelicidin: correlation between structural variations and antimicrobial activity, J. Biol. Chem. 281 (2006) 19861–19871.
[35] U.H.N. Dürr, U.S. Sudheendra, A. Ramamoorthy, LL-37, the only human member of the cathelicidin family of antimicrobial peptides, Biochim. Biophys. Acta 1758 (2006) 1408–1425.
[36] J.H. Kang, S.Y. Shin, S.Y. Jang, K.L. Kim, K.S. Hahm, Effects of tryptophan residues of porcine myeloid antibacterial peptide PMAP-23 on antibiotic activity, Biochem. Biophys. Res. Commun. 264 (1999) 281–286.
[37] D.G. Lee, D.H. Kim, Y. Park, H.K. Kim, H.N. Kim, Y.K. Shin, C.H. Choi, K.S. Hahm, Fungicidal effect of antimicrobial peptide, PMAP-23, isolated from porcine myeloid against Candida albicans, Biochem. Biophys. Res. Comm. 282 (2001) 570–574.
[38] K. Park, D. Oh, S.Y. Shin, K.S. Hahm, Y. Kim, Structural studies of porcine myeloid antibacterial peptide PMAP-23 and its analogues in DPC micelles by NMR spectroscopy, Biochem. Biophys. Res. Comm. 290 (2002) 204–212.
[39] S.T. Yang, J.H. Jeon, Y. Kim, S.Y. Shin, K.S. Hahm, J.I. Kim, Possible role of a PXXP central hinge in the antibacterial activity and membrane interaction of PMAP-23, a member of cathelicidin family, Biochemistry 45 (2006) 1775–1784.
[40] R.B. Merrifield, Solid-phase synthesis, Science 232 (1986) 341–347.
[41] J.C. McIntyre, R.G. Sleight, Fluorescence assay for phospholipid membrane asymmetry, Biochemistry 30 (1991) 11819–11827.
[42] K. Matsuzaki, O. Murase, N. Fujii, K. Miyajima, An antimicrobial peptide, magainin 2, induced rapid flip-flop of phospholipids coupled with pore formation and peptide translocation, Biochemistry 35 (1996) 11361–11368.
[43] A. Chattopadhyay, E. London, Parallax method for direct measurement of membrane penetration depth utilizing fluorescence quenching by spin-labeled phospholipids, Biochemistry 26 (1987) 39–45.
[44] L. Stella, V. Pallottini, S. Moreno, S. Leoni, F. De Maria, P. Turella, G. Federici, R. Fabrini, K.F. Dawood, M. Lo Bello, J.Z. Pedersen, G. Ricci, Electrostatic association of glutathione transferase to the nuclear membrane. Evidence of an enzyme defense barrier at the nuclear envelope, J. Biol. Chem. 282 (2007) 6372–6379.
[45] S. Esteban-Martín, J. Salgado, Self-assembling of peptide/membrane complexes by atomistic molecular dynamics simulations, Biophys. J. 92 (2007) 903–912.
[46] D.P. Tieleman, M.S.P. Sansom, H.J.C. Berendsen, Alamethicin helices in a bilayer and in solution: molecular dynamics simulations, Biophys. J. 76 (1999) 40–49.
[47] D. van der Spoel, E. Lindahl, B. Hess, G. Groenhof, A.E. Mark, H.J.C. Berendsen, GROMACS: fast, flexible and free, J. Comp. Chem. 26 (2005) 1701–1718.
[48] H.J.C. Berendsen, J.M. Postma, W.F. van Gunsteren, J. Hermans, Interaction models for water in relation to protein hydration, in: B. Pullman (Ed.), Intermolecular Forces, Reidel Publishing Company, Dordrecht, 1981, pp. 331–342.
[49] S. Miyamoto, P.A. Kollman, SETTLE: an analytical version of the SHAKE and RATTLE algorithms for rigid water models, J. Comp. Chem. 13 (1992) 952–962.
[50] O. Berger, O. Edholm, F. Jähnig, Molecular dynamics simulations of a fluid bilayer of dipalmitoylphosphatidylcholine at full hydration, constant pressure, and constant temperature, Biophys. J. 72 (1997) 2002–2013.
[51] S.J. Marrink, O. Berger, D.P. Tieleman, F. Jaehnig, Adhesion forces of lipids in a phospholipid membrane studied by molecular dynamics simulations, Biophys. J. 74 (1998) 931–943.
[52] W. Zhao, T. Róg, A.A. Gurtovenko, I. Vattulainen, M. Karttunen, Atomic-scale structure and electrostatics of anionic palmitoyloleoylphosphatidylglycerol lipid bilayers with Na^+ counterions, Biophys. J. 92 (2007) 1114–1124.
[53] H.J.C. Berendsen, J.P.M. Postma, W.F. van Gunsteren, A. Di Nola, J.R. Haak, Molecular dynamics with coupling to an external bath, J. Chem. Phys. 81 (1984) 3684–3690.
[54] B. Hess, H. Bekker, H.J.C. Berendsen, J.G.E.M. Fraaije, LINCS: a linear constraint solver for molecular simulations, J. Comp. Chem. 18 (1997) 1463–1472.
[55] T. Darden, D. York, L. Pedersen, Particle mesh Ewald: an N-log(N) method for Ewald sums in large systems, J. Chem. Phys. 98 (1993) 10089–10092.
[56] U. Essmann, L. Perera, M.L. Berkowitz, T. Darden, H. Lee, L.G. Pedersen, A smooth particle mesh Ewald potential, J. Chem. Phys. 103 (1995) 8577–8592.
[57] K.A. Feenstra, B. Hess, H.J.C. Berendsen, Improving efficiency of large time-scale molecular dynamics simulations of hydrogen-rich systems, J. Comp. Chem. 20 (1999) 786–798.
[58] W. Humphrey, A. Dalke, K. Shulten, VMD-visual molecular dynamics, J. Mol. Graph. 14 (1996) 33–38.
[59] A.S. Ladokhin, W.C. Wimley, K. Hristova, S.H. White, Mechanism of leakage contents of membrane vesicles determined by fluorescence requenching, Methods Enzymol. 278 (1997) 474–486.
[60] J.N. Weinstein, R.D. Klausner, T. Innerarity, E. Ralston, R. Blumenthal, Phase transition release, a new approach to the interaction of proteins with lipid vesicles, Biochim. Biophys. Acta 647 (1981) 270–284.

[61] G. Schwarz, A. Arbuzova, Pore kinetics reflected in the dequenching of a lipid vesicle entrapped fluorescent dye, Biochim. Biophys. Acta 1239 (1995) 51–57.
[62] R.F. Chen, J.R. Knutson, Mechanism of fluorescence concentration quenching of carboxyfluorescein in liposomes: energy transfer to nonfluorescent dimers, Anal. Biochem. 172 (1988) 61–77.
[63] K. Matsuzaki, O. Murase, N. Fujii, K. Miyajima, An antimicrobial peptide, magainin 2, induced rapid flip-flop of phospholipids coupled with pore formation and peptide translocation, Biochemistry 35 (1996) 11361–11368.
[64] J.C. McIntyre, R.G. Sleight, Fluorescence assay for phospholipid membrane asymmetry, Biochemistry 30 (1991) 11819–11827.
[65] A.S. Ladokhin, Analysis of protein and peptide penetration into membranes by depth-dependent fluorescence quenching: theoretical considerations, Biophys. J. 76 (1999) 946–955.
[66] A.S. Ladokhin, Distribution analysis of depth-dependent fluorescence quenching in membranes: a practical guide, Meth. Enzymol. 278 (1997) 462–473.
[67] K.P. Voges, G. Jung, W.H. Sawyer, Depth-dependent fluorescent quenching of a tryptophan residue located at defined positions on a rigid 21-peptide helix in liposomes, Biochim. Biophys. Acta 896 (1987) 64–76.
[68] A.S. Ladokhin, Evaluation of lipid exposure of tryptophan residues in membrane peptides and proteins, Anal. Biochem. 276 (1999) 65–71.
[69] E. Glukhov, M. Stark, L.L. Burrows, C.M. Deber, Basis for selectivity of cationic antimicrobial peptides for bacterial versus mammalian membranes, J. Biol. Chem. 280 (2005) 33960–33967.
[70] J.W. Nichols, Phospholipid transfer between phosphatidylcholine-taurocholate mixed micelles, Biochemistry 27 (1989) 3925–3931.
[71] B. Pispisa, C. Mazzuca, A. Palleschi, L. Stella, M. Venanzi, F. Formaggio, C. Toniolo, Q.B. Broxterman, Structural features and conformational equilibria of 3_{10}-helical peptides in solution by spectroscopic and molecular mechanics studies, Biopolymers 67 (2002) 247–250.
[72] B. Pispisa, C. Mazzuca, A. Palleschi, L. Stella, M. Venanzi, M. Wakselman, J.P. Mazaleyrat, M. Rainaldi, F. Formaggio, C. Toniolo, A combined spectroscopic and theoretical study of a series of conformationally restricted hexapeptides carrying a rigid binaphthyl-nitroxide donor-acceptor pair, Chem. Eur. J. 9 (2003) 2–11.
[73] L.J. Lis, M. McAlister, N.L. Fuller, R.P. Rand, V.A. Parsegian, Measurement of the lateral compressibility of several phospholipid bilayers, Biophys. J. 37 (1982) 667–672.
[74] D.E. Wolf, A.P. Winiski, A.E. Ting, K.M. Bocian, R.E. Pagano, Determination of the transbilayer distribution of fluorescent lipid analogues by nonradiative fluorescence resonance energy transfer, Biochemistry 31 (1982) 2865–2873.
[75] F.S. Abrams, E. London, Extension of the parallax analysis of membrane penetration depth to the polar region of model membranes: use of fluorescence quenching by a spin-label attached to the phospholipid polar headgroup, Biochemistry 32 (1993) 10826–10831.
[76] S. Mazeres, V. Schram, J.F. Tocanne, A. Lopez, 7-Nitrobenz-2-oxa-1,3-diazole-4-yl-labeled phospholipids in lipid membranes: differences in fluorescence behavior, Biophys. J. 71 (1996) 327–335.
[77] C.L. Wee, D. Gavaghan, M.S.P. Sansom, Lipid bilayer deformation and the free energy of interaction of a Kv channel gating-modifier toxin, Biophys. J. 95 (2008) 3816–3826.
[78] T. Carpenter, P.J. Bond, S. Khalid, M.S.P. Sansom, Self-assembly of a simple membrane protein: coarse grained molecular dynamics simulations of the influenza M2 channel, Biophys. J. 95 (2008) 3790–3801.
[79] S.J. Marrink, E. Lindhal, O. Edholm, A.E. Mark, Simulation of the spontaneous aggregation of phospholipids into bilayers, J. Am. Chem. Soc. 123 (2001) 8638–8639.
[80] A.H. de Vries, A.E. Mark, S.J. Marrink, Molecular dynamics simulation of the spontaneous formation of a small dppc vesicle in water in atomistic detail, J. Am. Chem. Soc. 126 (2004) 4488–4489.
[81] H. Leontiadou, A.E. Mark, S.J. Marrink, Molecular dynamics simulations of hydrophilic pores in lipid bilayers, Biophys. J. 86 (2004) 2156–2164.
[82] E. Egberts, S.J. Marrink, H.J. Berendsen, Molecular dynamics simulation of a phospholipid membrane, Eur. Biophys. J. 22 (1994) 423–436.
[83] R. Fischer, M. Fotin-Mleczek, H. Hufnagel, R. Brock, Break on through to the other side — biophysics and cell biology shed light on cell-penetrating peptides, ChemBioChem 6 (2005) 2126–2142.
[84] R.M. Epand, Fusion peptides and the mechanism of viral fusion, Biochim. Biophys. Acta 1614 (2003) 116–121.
[85] L.A. Munishkina, A.L. Fink, Fluorescence as a method to reveal structures and membrane-interactions of amyloidogenic proteins, Biochim. Biophys. Acta 1768 (2007) 1862–1885.
[86] P. Raman, V. Cherezova, M. Caffrey, The membrane protein data bank, Cell Mol. Life Sci. 63 (2006) 36–51.
[87] B. Pispisa, A. Palleschi, C. Mazzuca, L. Stella, A. Valeri, M. Venanzi, F. Formaggio, C. Toniolo, Q.B. Broxterman, The versatility of combining FRET measurements and molecular mechanics results for determining the structural features of ordered peptides in solution, J. Fluoresc. 12 (2002) 213–217.
[88] M. Venanzi, A. Valeri, A. Palleschi, L. Stella, L. Moroder, F. Formaggio, C. Toniolo, B. Pispisa, Structural properties and photophysical behavior of conformationally constrained hexapeptides functionalized with a new fluorescent analog of tryptophan and a nitroxide radical quencher, Biopolymers 75 (2004) 128–139.
[89] M. Venanzi, E. Gatto, G. Bocchinfuso, A. Palleschi, L. Stella, F. Formaggio, C. Toniolo, Dynamics of formation of a helix-turn-helix structure in a membrane-active peptide: a time-resolved spectroscopic study, ChemBioChem 7 (2006) 43–45.
[90] L. Stella, G. Bocchinfuso, E. Gatto, C. Mazzuca, M. Venanzi, F. Formaggio, C. Toniolo, A. Palleschi, B. Pispisa. Peptide foldamers: from spectroscopic studies to applications. In Reviews in Fluorescence. C. D. Geddes and J. R. Lakowicz (Eds.), Springer, New York. In press.
[91] L. Stella, A. Caccuri, N. Rosato, M. Nicotra, M. Lo Bello, F. De Matteis, A.P. Mazzetti, G. Federici, G. Ricci, Flexibility of helix 2 in the human glutathione transferase P1-1: time-resolved fluorescence spectroscopy, J. Biol. Chem. 273 (1998) 23267–23273.
[92] L. Stella, M. Nicotra, G. Ricci, N. Rosato, E.E. Di Iorio, Molecular dynamics simulations of human glutathione transferase P1-1: analysis of the induced-fit mechanism by GSH binding, Proteins 37 (1999) 1–9.
[93] L. Stella, E.E. Di Iorio, M. Nicotra, G. Ricci, Molecular dynamics simulations of human glutathione transferase P1-1: conformational fluctuations of the apo-structure, Proteins 37 (1999) 10–19.
[94] S.S. Antollini, Y. Xu, H. Jiang, F.J. Barrantes, Fluorescence and molecular dynamics studies of the acetylcholine receptor γM4 transmembrane peptide in reconstituted systems, Mol. Membr. Biol. 22 (2005) 471–483.
[95] K.P. Voges, G. Jung, W.H. Sawyer, Depth dependent fluorescent quenching of a tryptophan residue located at defined positions on a rigid 21-peptide helix in liposomes, Biochim. Biophys. Acta 896 (1987) 64–76.
[96] B. de Foresta, L. Tortech, M. Vincent, J. Gallay, Location and dynamics of tryptophan in transmembrane a-helix peptides: a fluorescence and circular dichroism study, Eur. Biophys. J. 31 (2002) 185–197.
[97] K.A. Henzler Wildman, D.K. Lee, A. Ramamoorthy, Mechanism of lipid bilayer disruption by the human antimicrobial peptide, LL-37, Biochemistry 42 (2003) 6545–6558.
[98] K.A. Henzler Wildman, G.V. Martinez, M.F. Brown, A. Ramamoorthy, Perturbation of the hydrophobic core of lipid bilayers by the human antimicrobial peptide LL-37, Biochemistry 43 (2004) 8459–8469.
[99] M. Fernández-Vidal, S. Jayasinghe, A.S. Ladokhin, S.H. White, Folding amphipathic helices into membranes: amphiphilicity trumps hydrophobicity, J. Mol. Biol. 370 (2007) 459–470.
[100] V. Dhople, A. Krukemeyer, A. Ramamoorthy, The human beta-defensin-3, an antibacterial peptide with multiple biological functions, Biochim. Biophys. Acta 1758 (2006) 1499–1512.
[101] J.L. MacCallum, W.F. Drew Bennet, D.P. Tieleman, Partitioning of amino acid side chains into lipid bilayers: results from computer simulations and comparison to experiment, J. Gen. Physiol. 129 (2007) 371–377.
[102] R. Wolfenden, Experimental measures of amino acid hydrophobicity and the topology of transmembrane and globular proteins, J. Gen. Physiol. 129 (2007) 357–362.
[103] S.H. White, W.C. Wimley, Membrane protein folding and stability: physical principles, Annu. Rev. Biophys. Biomol. Struct. 28 (1999) 319–365.
[104] T. Hessa, H. Kim, K. Bihlmaier, C. Lundin, J. Boekel, H. Andersson, I. Nilsson, S. H White, G. von Heijne, Recognition of transmembrane helices by the endoplasmic reticulum translocon, Nature 433 (2005) 377–381.
[105] J.A. Freites, D.J. Tobias, G. von Heijne, S.H. White, Interface connections of a transmembrane voltage sensor, Proc. Natl. Acad. Sci. U. S. A. 102 (2005) 15059–15064.
[106] S. Dorairaj, T.W. Allen, On the thermodynamic stability of a charged arginine side chain in a transmembrane helix, Proc. Natl. Acad. Sci. U. S. A. 104 (2007) 4943–4948.
[107] H.D. Herce, A.E. Garcia, Molecular dynamics simulations suggest a mechanism for translocation of the HIV-1 TAT peptide across lipid membranes, Proc. Natl. Acad. Sci. U. S. A. 104 (2007) 20805–20810.
[108] A.C.V. Johansson, E. Lindhal, Position-resolved free energy of solvation for amino acids in lipid membranes from molecular dynamics simulations, Proteins 70 (2008) 1332–1344.
[109] J. Yoo, Q. Cui, Does arginin remain protonated in the lipid membrane? Insights from microscopic pKa calculations, Biophys. J. 94 (2008) L61–L63.
[110] L. Li, I. Vorobyov, T.W. Allen, Potential of mean force and pKa profile calculation for a lipid membrane-exposed arginine side chain, J. Phys. Chem. B 112 (2008) 9574–9587.
[111] L. Li, I. Vorobyov, A.D. MacKerell Jr., T.W. Allen, Is arginine charged in a membrane? Biophys. J. 94 (2008) L11–L13.
[112] W.C. Wimley, K. Gawrisch, T.P. Creamer, S.H. White, Direct measurement of salt-bridge solvation energies using a peptide model system: implications for protein stability, Proc. Natl. Acad. Sci. U. S. A. 93 (1996) 2985–2990.
[113] L. Yang, T.A. Harroun, T.M. Weiss, L. Ding, H.W. Huang, Barrel-stave model or toroidal model? A case study on melittin pores, Biophys. J 81 (2001) 1475–1485.
[114] G. Baumann, P. Mueller, A molecular model of membrane excitability, J. Supramol. Struct. 2 (1974) 538–557.
[115] Y. Shai, Mechanism of the binding, insertion and destabilization of phospholipid bilayer membranes by α-helical antimicrobial and cell non-selective membrane-lytic peptides, Biochim. Biophys. Acta 1462 (1999) 55–70.
[116] K. Matsuzaki, Why and how are peptide–lipid interactions utilized for self-defense? Magainins and tachyplesins as archetypes, Biochim. Biophys. Acta 1462 (1999) 1–10.
[117] L. Yang, T.M. Weiss, R.I. Lehrer, H.W. Huang, Crystallization of antimicrobial pores in membranes: magainin and protegrin, Biophys. J. 79 (2000) 2002–2009.
[118] S.J. Ludtke, K. He, W.T. Heller, T.A. Harroun, L. Yang, H.W. Huang, Membrane pores induced by magainin, Biochemistry 35 (1997) 13723–13728.
[119] H.W. Huang, Action of antimicrobial peptides: two-state model, Biochemistry 39 (2000) 8347–8352.
[120] M. Tang, A.J. Waring, M. Hong, Phosphate-mediated arginine insertion into lipid membranes and pore formation by a cationic membrane peptide from solid-state NMR, J. Am. Chem. Soc. 129 (2007) 11438–11446.
[121] V.A. Parsegian, N. Fuller, R.P. Rand, Measured work of deformation and repulsion of lecithin bilayers, Proc. Natl. Acad. Sci. U. S. A. 76 (1979) 2750–2754.